Journal of Science and Technology ‒ Smart Systems and Devices
Volume 36, Issue 3, September 2026, 038–047

Thermal Effects of Harmonics on Distribution Transformers: A Coupled Electromagnetic–Thermal Finite-Element-Based Approach

Loi Tran Van[1], Thao Ho Nguyen[1], Trung Ho Van[1], Bao Doan Thanh[2], Duong Le Dinh[1], Anh Nguyen Kim [1,*]
[1]University of Science and Technology, The University of Danang, Da Nang, Vietnam
[2] Faculty of Engineering and Technology, Quy Nhon University, Gia Lai, Vietnam
[*]Corresponding author email: nkanh@dut.udn.vn

Abstract

The growing demand for electrical energy, together with increasingly complex operating conditions caused by nonlinear loads and the widespread integration of renewable energy sources, has led to increased harmonic distortion in power systems. As critical assets in distribution networks, transformers are particularly vulnerable to harmonic-induced losses and thermal stress, which can accelerate insulation aging and reduce service life. This study investigates the thermal effects of harmonics on a medium-voltage distribution transformer using a coupled electromagnetic–thermal approach based on the finite element method. In the proposed workflow, ANSYS Maxwell is used to compute electromagnetic quantities and harmonic-dependent losses, and these losses are then used as inputs to an equivalent electro-thermal model to predict top-oil and winding hot-spot temperatures. The electromagnetic model is validated under no-load and short-circuit conditions, and simulations are conducted for linear and nonlinear loads at 50%, 100%, and 125% of rated load. The hybrid thermal prediction results show good agreement with detailed ANSYS Mechanical simulations, with a deviation of approximately 3% in the linear-load case and 0.016% in the nonlinear-load case. The results show that harmonic loading significantly increases load-related losses and hot-spot temperature, while also revealing a non-uniform temperature distribution that enables hot-spot localization. The obtained spatial hot-spot information supports insulation loss-of-life assessment and provides practical guidance for design improvement, sensor placement, periodic inspection/testing, spare-part planning, and condition-based maintenance under harmonic operating conditions.

Keywords: Current harmonics, electromagnetic-thermal modeling, finite element method, medium-voltage transformer, thermal behavior.

1. Introduction

Power transformers are essential elements in electrical power distribution networks [1]. Similar to all devices, transformers are subject to aging, and the dominant factor in this regard is the loss-dependent temperature [2]. In recent studies, transformer aging and insulation degradation have been shown to be closely associated with thermally driven electrical and electro-thermal fault mechanisms, which can be effectively identified through dissolved gas analysis and data-driven diagnostic models [3, 4]. Such loss-induced heating is minimized when the transformer operates at the nominal system frequency (50 Hz) with sinusoidal voltage and current waveforms. However, the growing penetration of converters, hybrid configurations, and nonlinear loads result in high-level harmonic parameters. Consequently, the waveforms of the current and voltage become distorted and are no longer purely sinusoidal. These harmonics affect both the amplitude and the frequency spectrum of the transformer [5]. High harmonic amplitudes contribute to higher I^2R losses, elevated thermal stress, and a decline in transformer efficiency. Furthermore, the appearance of high-order frequency h (5^{th}, 7^{th}, 11^{th}, 13^{th}, 17^{th}, 19^{th}, etc.) is directly proportional not only to power losses in core (hysteresis loss, eddy loss and excessive loss) [6], but also to eddy-current loss ($P_{EC} \sim h^2$) and other stray loss ($P_{OSL} \sim h^{0.8}$) in the winding. Consequently, the transformer generally reaches higher temperatures, particularly in the parts, where the hot-spot temperature is critical with respect to the temperature-dependent lifetime duration of the transformer [2].

Considering the cost and importance of the transformer, one must build a model to calculate the power loss and predict the transformer temperature in the presence of harmonics. This will facilitate the identification of transformers requiring maintenance and contribute to maintaining power distribution stability.

Among the models for predicting transformer lifespan, the thermal model is the most widely accepted and used by scientific organizations such as IEC and IEEE. By simplifying complex systems into equivalent electro-thermal models using RC circuits,

p-ISSN 3093-3285
e-ISSN 3093-3315
https://doi.org/10.51316/jst.192.ssad.2026.36.3.5.
Received: Dec 26, 2025; Revised: Mar 29, 2026;
Accepted: Apr 8, 2026; Online: May 27, 2026

thermal models can predict the increase in oil peak temperature, the temperature on the windings, and especially, the appearance of hot-spots [7]. With temperature models, the two most common methods are circuit-based models and numerical methods [8–10]. Circuit-based models have the advantage of being easy to implement, flexible, and applicable to many types of transformers [8-9]. The authors of work [8] created a thermal model to calculate top-oil and hot-spot temperatures for distribution transformers without external cooling. The most important contribution is that the authors considered the nonlinearity of the oil and winding resistance, which improved the accuracy of the calculation model when operating under various load conditions. Work [9] further extended the model to calculate oil temperature and hot-spot temperature on the windings under the operating conditions of transformers transmitting nonlinear loads. However, the drawback of this model is that it cannot provide a comprehensive view of the loss and temperature distribution of the internal components of the transformer because of the assumption of a uniform temperature distribution in the oil.

The second method overcomes the drawback of the previous method by providing a picture of the processes occurring in the transformer, such as the temperature distribution, fluid velocity field, and hot-spot location [10-11]. In [10], core losses and flux distribution were obtained using Finite Element Method (FEM), and the resulting loss data were subsequently incorporated into an equivalent circuit in MULTISIM to evaluate the transformer's thermal behavior. The results obtained from the model compared with actual measurements showed a small error of approximately 2°C for winding temperature and 4°C for oil temperature. In [11], a three-dimensional (3D) model linking the electric field, fluid flow, and temperature was established. The loss data obtained from FEM were then used as inputs to solve the mass- and momentum-conservation equations using the Finite Volume Method (FVM), enabling the prediction of the flow field and the resulting non-uniform temperature distribution within the transformer. The reported errors between simulation and measurements are below 3°C.

However, a significant drawback of numerical methods is their dependence on comprehensive input data and high computational requirements, often requiring powerful hardware and long simulation times; moreover, model setup can be complex. Therefore, to address these limitations, this study improves the determination of input parameters. Instead of relying on theoretical or rated loss values, a 3D FEM model in ANSYS Maxwell is used to extract accurate local loss data under harmonic conditions. The resulting outputs (e.g., currents, loss components, and hot-spot losses) are then used as inputs to the differential equations of the equivalent electro-thermal circuit model. This hybrid framework balances accuracy and computational cost: whereas a full 3D FEM thermal simulation is time-consuming, solving the electro-thermal differential equations in MATLAB/Simulink (Runge–Kutta) supports efficient, potentially real-time monitoring. Finally, this approach goes beyond temperature prediction by integrating IEC 60076-7 to directly assess insulation loss of life, providing a more comprehensive view of transformer reliability in modern power-grid environments.

The ANSYS model was validated under various operating conditions, including no-load and short-circuit tests. Simulations are performed for both linear and nonlinear loading at 50%, 100%, and 125% of rated load. The results demonstrate the severe impact of harmonics on the top-oil temperature and the winding hot-spot temperature. In addition, the winding region with the maximum loss is identified using field plots in ANSYS Maxwell and ANSYS Mechanical, which is consistent with the hot-spot location on the coil. In this study, the nonlinear load is modeled as a DC motor drive consisting of a DC motor–equivalent RL load fed by a three-phase controlled rectifier; the rectifier operation (e.g., firing-angle control) injects harmonic currents into the transformer.

The remainder of this paper is organized as follows. Section 2 presents the theoretical background and methodology, including the analysis of harmonic-induced losses in transformers and the implementation of a coupled electromagnetic–thermal model. Section 3 describes the finite element modeling of the medium-voltage distribution transformer and discusses the validation of the proposed model under various operating conditions. The simulation results, including power losses, temperature rise, hot-spot behavior, and insulation loss of life under harmonic and non-harmonic loads, are analyzed and discussed in this section. Finally, Section 4 concludes the paper and outlines the main findings and limitations of the study, along with perspectives for future research.

2. Methodology

2.1. Loss Computation Using Finite Element Method

For sinusoidal steady-state electromagnetic analysis at angular frequency ω, Maxwell's equations can be written in the frequency domain as follows [12]:

$$\nabla \times \frac{1}{\mu} B = \sigma E + j\varepsilon\omega E \tag{1}$$

$$\nabla \times E = -j\omega B \tag{2}$$

$$\nabla.\varepsilon E = \rho \quad (3)$$

$$\nabla.\mu H = 0 \quad (4)$$

where, E is the electric field strength [V/m]; B is the magnetic flux density [T]; H is the magnetic field strength [A/m]; ρ is the charge density [C/m^3]; ε is the electric permittivity [F/m]; μ is the permeability [H/m]; and σ is the electrical conductivity [S/m].

Solving Maxwell's equation requires using the vector potential A and the electric potential ϕ. The scalar potential can be used to describe an external voltage or current in a conductor and is defined by:

$$\nabla \times \frac{1}{\mu}(\nabla \times A) = (\sigma + j\varepsilon\omega)(-j\omega A - \nabla\phi) \quad (5)$$

The total current flowing through a conductor is given by the integral of the current density over a cross-sectional area Ω.

$$I_T = I_s + I_{ec} + I_d = \int_\Omega (\sigma + j\varepsilon\omega)(-j\omega A - \nabla\phi) d\Omega \quad (6)$$

I_s denotes the current supplied by an external source, expressed as:

$$I_s = \int_\Omega -\sigma\nabla\phi \, d\Omega \quad (7)$$

I_{ec} is the induced eddy-current, given by:

$$I_{ec} = \int_\Omega -j\omega\sigma A \, d\Omega \quad (8)$$

And I_d is the displacement current:

$$I_d = \int_\Omega -j\varepsilon\omega(j\omega A + \nabla\phi) \, d\Omega \quad (9)$$

Equations (5) and (6) are fundamental for calculating A and ϕ, which are subsequently used to determine variables such as B, E, and J. Consequently, the loss values of the transformer can be determined. The losses per unit length of the conductor are computed by integrating the loss density over the cross-section and assembling the finite-element contributions e, as follows:

$$P_W = \iint_S \frac{1}{\sigma}(J_s^2 + J_{ec}^2) dS = \sum_e \frac{1}{\sigma}(J_s^2 + J_{ec}^2)\,\Omega_e \quad (10)$$

2.2. Effects of Harmonics on Losses in Transformers

Transformer losses are generally classified as no-load loss P_{NL} and load loss P_{LL}. P_{NL} in a power transformer primarily comprises core losses resulting from induced eddy currents and magnetic hysteresis during core magnetization. These losses are dependent on the frequency, amplitude, and waveform of the excitation voltage [6]:

$$P_{NL} = \sum_n (k_h f_h B_{n,peak}^{\alpha} + k_e f_h^2 B_{n,peak}^2 + k_a f_h^{1.5} B_{n,peak}^{1.5}) \quad (11)$$

where $f_h = hf_1$ is the frequency of the h^{th} harmonic considered, f_1 = 50 Hz is the fundamental frequency, and $B_{n,peak}$ is the peak value of the magnetic flux density due to h^{th} harmonic. The terms k_h, k_e, k_a, and α were determined using core steel sheet data [6].

P_{LL} is subdivided into P_{dc} losses (I^2R_{dc}), winding eddy-current losses P_{EC} and other stray losses P_{OSL} . The total load-loss equation is given in [5]:

$$P_{LL} = P_{dc} + P_{EC} + P_{OSL} \quad (12)$$

Under sinusoidal current waveform conditions, P_{dc} can be calculated by multiplying the resistance winding R_{dc} with the square of the load current I_{RMS}^2. Under harmonic waveform conditions, P_{dc} can be calculated [13]:

$$P_{dc} = P_{dc-R} \sum_{h=1}^{h=max} \frac{I_h^2}{I_R^2} \quad (13)$$

where P_{dc-R} is the resistance loss at the rated load current I_R [W]; I_h is related to the current at harmonic order h [A]; h is the harmonic order.

Based on the IEEE C57.110-2018 standard, the eddy-current losses P_{EC} in the winding caused by the generated magnetic flux are considered to vary according to the square of the RMS current and the square of the harmonic frequency:

$$P_{EC} = P_{EC-R} \frac{\sum_{h=1}^{h=max} h^2 I_h^2}{I_R^2} \quad (14)$$

where P_{EC-R} is the eddy-current loss at rated load [W].

Other stray losses are a component of eddy-current losses generated in the structural components of the transformer due to induced currents, excluding windings [5]. Several factors contribute, like the core size, transformer voltage level, structural materials used in the tank, and the effect of harmonic currents that cause rise losses [13]:

$$P_{OSL} = P_{OSL-R} \sum_{h=1}^{h=max} h^{0.8} \frac{I_h^2}{I_R^2} \quad (15)$$

where P_{OSL-R} is the other stray loss at rated load [W].

These increased losses raise the temperature of the transformer compared to when a pure sine wave is applied, as mentioned in Section 2.2. Therefore, it is necessary to determine the increased losses caused by using ANSYS Maxwell software.

2.3. Transformer Thermal Model

Owing to uneven temperature distribution, the part working at the highest temperature often deteriorates the most. Therefore, the aging rate is referenced based on the hot-spot temperature of the winding [14]. To analyze the temperature of the transformer, a simple equivalent circuit representing the thermal flow equations for the transformer is shown in Table 1. The model is characterized by using an equivalent current source to represent the heat generated by losses, and a nonlinear equivalent resistor to represent the effect of convective cooling by air or oil [15].

The electrical equations of the equivalent circuit can be expressed as:

$$v = R_{el} i \text{ and } i = C_{el} \frac{dv}{dt} \tag{16}$$

The corresponding thermal laws are:

$$\theta = R_{th} q \text{ and } q = C_{th} \frac{d\theta}{dt} \tag{17}$$

Table 1. Parameter of thermal-electrical equivalent model

Thermal	Electrical
Heat transfer rate q [W]	Current i [A]
Temperature θ [°C]	Voltage v [V]
Thermal resistance R_{th} [°C/W]	Resistance R_{el} [Ω]
Thermal capacitance C_{th} [$Joules$/°C]	Capacitance C_{el} [F]

The analogy between the heat transfer process and the charge-discharge process of an electrical circuit is reflected in the capacitor element C. Capacitance C_{el} stores the electrical energy, and thermal capacitance C_{th} stores heat energy, such as in oil.

To use this model, it is necessary to assume that the temperature distribution in the medium (oil) is uniform at any given time. Next, the Biot number (Bi) is calculated, which is defined as the ratio between the thermal resistance of the oil and the thermal resistance of the air. Swift assumes that the temperature in the oil is uniform at all times, or it is known as the "*lumped capacitance*" model. This is reasonable for transformer oil because the internal thermal resistance of the object (oil) is considerably lower than the surface thermal resistance (air). Therefore, $Bi = \frac{R_{oil}}{R_{air}} \ll 1$ and in this research, the temperature within the oil can be considered uniform.

2.3.1. Oil-to-air model

In the thermal and equivalent-circuit models shown in Figs. 1 and 2 [15], all losses are represented as heat sources supplied to the system.

The differential equation for the equivalent circuit, as follows [15]:

$$q_{Fe} + q_{Cu} = C_{th-oil} \frac{d\theta_{oil}}{dt} + \frac{[\theta_{oil} - \theta_{amb}]^{1/n}}{R_{th-oil}} \tag{18}$$

Where q_{Fe} is the heat generated by P_{NL} [W]; q_{Cu} is the heat produced by P_{LL} [W]; C_{th-oil} is combined into a single equivalent capacitor [W.min/°C]; R_{th-oil} represents the equivalent thermal resistance of the oil [°C/W]; θ_{amb} is the ambient temp [°C]; θ_{oil} is the top-oil temp [°C]; and n is the cooling constant [17].

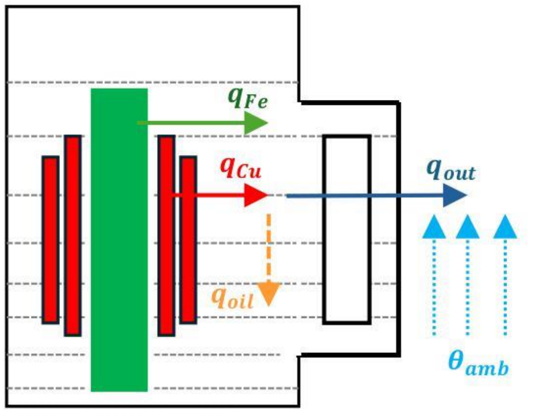

Fig. 1. Thermal representation of heat transfer from oil to ambient air

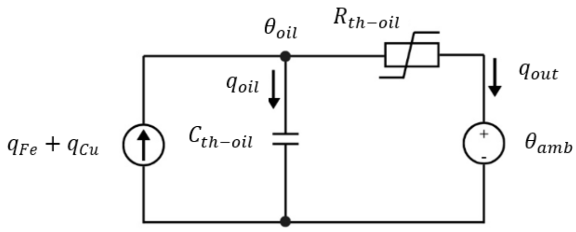

Fig. 2. Electrical-thermal equivalent circuit

From (18), we have:

$$\frac{P_{NL-H} + P_{LL-H}}{P_{NL-H} + P_{LL-R}} [\Delta\theta_{oilR}]^{\frac{1}{n}} = \tau_{oil} \frac{d\theta_{oil}}{dt} + [\theta_{oil} - \theta_{amb}]^{\frac{1}{n}} \tag{19}$$

Here, $\tau_{oil} = C_{th-oil} R_{th-oil}$ denotes the top oil time constant [min], while $\Delta\theta_{oilR}$ represents the rated top-oil temperature rise above the ambient level [K].

Following (13), (14), and (15), the load loss P_{LL-H} at the harmonic load which is equal to:

$$P_{dc-R} \sum_{h=1}^{max} \frac{I_h^2}{I_R^2} + P_{EC-R} \frac{\sum_{h=1}^{max} \mathrm{h}^2 I_h^2}{I_R^2} + P_{OSL-R} \sum_{h=1}^{max} \mathrm{h}^{0.8} \frac{I_h^2}{I_R^2} \tag{20}$$

The equation calculates the top oil temperature using Eqs. (9) and (10):

$$D\theta_{oil} = \frac{Dt}{\tau_{oil}} \left[\frac{P_{NL-H} + P_{LL-H}}{P_{NL-R} + P_{LL-R}} [\Delta\theta_{oilR}]^{\frac{1}{n}} - [\theta_{oil} - \theta_{amb}]^{\frac{1}{n}} \right] \tag{21}$$

The top-oil temperature obtained from the oil-air thermal model is subsequently used as the ambient reference for the winding–oil model.

Journal of Science and Technology — Smart Systems and Devices
Volume 36, Issue 3, September 2026, 038–047

2.3.2. Winding-to-oil model

The heat transfer model from the winding to the oil is illustrated in Fig. 3, adapted from [15]. This model determines the hot-spot on the coil.

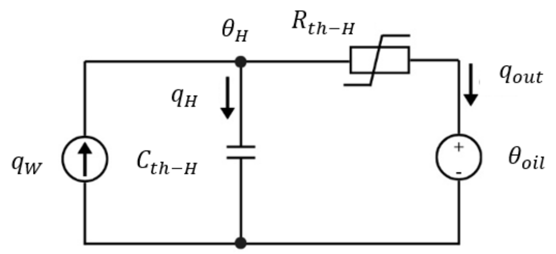

Fig. 3. Winding-to-oil model

From the thermal model of the winding to the oil, we establish the equation for the electrical-thermal equivalent circuit:

$$q_W = C_{th-H}\frac{d\theta_H}{dt} + \frac{1}{R_{th-H}}[\theta_H - \theta_{oil}]^{\frac{1}{m}} \tag{22}$$

With q_W is the heat created by coil loss at the hot-spot [W]; C_{th-H} is the capacitance of the hot-spot [W.min/°C]; R_{th-H} is the thermal resistance of the hot-spot under rated conditions [°C/W]; θ_H is the hot-spot temperature [°C]; and *m* is the cooling constant.

From (12), we have:

$$\frac{\sum_{h=1}^{max}\frac{I_h^2}{I_R^2} + P_{EC-H(pu)}\sum_{h=1}^{max}\frac{I_h^2}{I_R^2}}{1+P_{EC-R(pu)}}[\Delta\theta_{H-R}]^{\frac{1}{m}} = \tau_H\frac{d\theta_H}{dt} + [\theta_H - \theta_{oil}]^{\frac{1}{m}} \tag{23}$$

Where, P_{EC-H} is the per unit (p.u.) loss at the hot-spot location at the harmonic load; P_{EC-R} is the p.u loss at the hot-spot location at the rated load; τ_H represents the winding time constant at the hot-spot [min]; and $\Delta\theta_H$ indicates the temperature rise of the hot-spot relative to the top oil [K].

So hot-spot temperature is calculated:

$$D\theta_H = \frac{Dt}{\tau_H}\left[\frac{\sum_{h=1}^{max}\frac{I_h^2}{I_R^2} + P_{EC-H(pu)}\sum_{h=1}^{max}\frac{I_h^2}{I_R^2}}{1+P_{EC-R(pu)}}[\Delta\theta_{H-R}]^{\frac{1}{m}} - [\theta_H - \theta_{oil}]^{\frac{1}{m}}\right] \tag{24}$$

Using the same Runge–Kutta numerical method for differential (21) and (24), we can calculate the top-oil and hot-spot temp. These results are discussed in Section 3.3.

2.3.3. Loss of insulation life

IEC 60076-7 provides a method for assessing the insulation loss of life of a transformer based on θ_H. The relative ageing rate *V* is defined by (25).

$$V\,(\text{p.u.}) = e^{\left(\frac{15000}{383} - \frac{15000}{\theta_H + 273}\right)} \tag{25}$$

The per unit loss of life factor is:

$$L\,(\text{p.u.}) = \int_{t1}^{t2} e^{\left(\frac{15000}{383} - \frac{15000}{\theta_H + 273}\right)} dt \tag{26}$$

Predicting the reduced lifespan of a transformer allows for an assessment of the extent of damage to equipment operating under higher harmonic conditions.

3. Valid Model and Results

3.1. Transformer Thermal Model

3.1.1. Information of model

In this paper, an analysis distribution transformer (320 kVA, 35/0.4 kV) is modeled using ANSYS Maxwell software. The results are presented in Tables 2 and 3.

Table 2. Nominal electrical parameters of the transformer

Rated Power S_{rated}	**320 kVA**
Phase	3
Voltage	35 ± 2 x 2.5% / 0.4 kV
Frequency	50 Hz
Vector Group	Y_{y0} -12
No-load Losses P_0	385 W
No-load Current i_0%	2
Short Circuit Losses P_n	3170 W
Short-circuit voltage u_n%	4
Cooling	ONAN

Table 3. Winding and core dimensions of the transformer

High winding	
Material	Copper
Number of turns	2450
Height [mm]	345
Inner Diameter [mm]	263
Low winding	
Material	Copper
Number of turns	28
Height [mm]	375
Inner Diameter [mm]	182
Core	
Material	27GHJ100
Thickness [mm]	0.27
Length [mm]	830
Height [mm]	720
Type	4-step core limb and 3-step yoke core

3.1.2. Winding and magnetic circuit model of transformer

The electrical and geometrical design parameters of this transformer serve as the basis for constructing the model and performing simulations in ANSYS Maxwell. The simulation model is illustrated in Fig. 4.

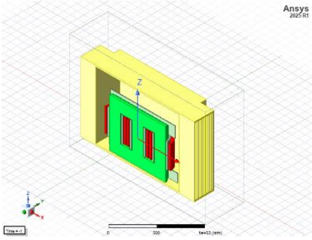

Fig. 4. Model of 35/0.4 kV transformer in ANSYS Maxwell

During the calculation and transient analysis in ANSYS Maxwell, the transformer is energized through an external excitation circuit created using ANSYS Twin Builder. The external excitation circuit is shown in Fig. 5.

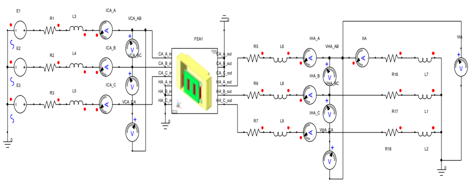

Fig. 5. External excitation circuit model

3.2. Valid Model

In this study, the simulation process incorporates several operating conditions to compare the obtained results with calculated data and to evaluate the model's reliability under practical operation. The operation modes considered include no-load, short-circuit, and load conditions, both with and without harmonic distortion.

3.2.1. No-load and short circuit simulation

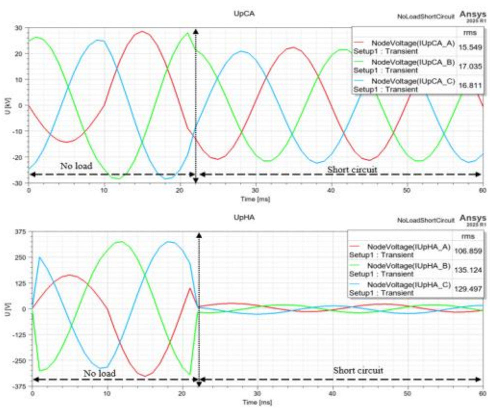

Fig. 6. Results of U_p under no-load and short-circuit conditions

During the no-load operation period, a high-voltage winding is supplied with the rated voltage. Meanwhile, the low-voltage winding is connected to a high-value resistor to simulate an open circuit. In the short-circuit stage, the low-voltage winding is shorted. The results for these two operating conditions are illustrated in Figs. 6 and 7, respectively.

In the no-load condition, $I_{pLV} \approx 0$ A and $U_{pLV} = 217.53$ V, exhibiting a deviation of 1.36% from the calculated value of 220 V, which falls within the acceptable tolerance range. In the short-circuit condition, $I_{pLV} = 3.93$ kA and $U_{Plv} = 21.81$ V, indicating high accuracy and good agreement with the practical short-circuit test results.

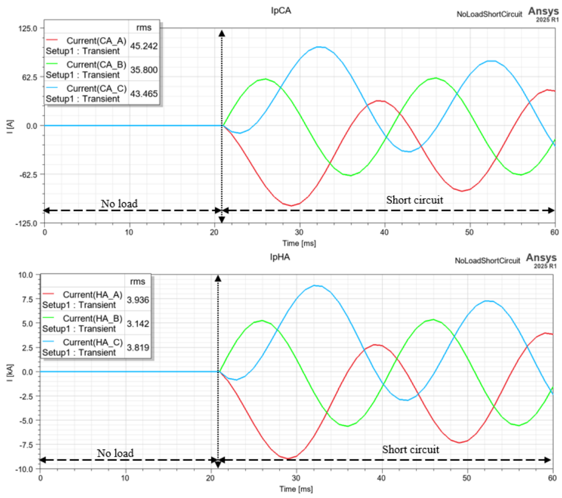

Fig. 7. Results of I_p under no-load and short-circuit conditions

3.2.2. Simulation load operation without harmonics

As shown in Table 4, under this condition without harmonic distortion, the simulation results exhibit deviations within the acceptable range compared with the calculated values.

Table 4. Comparison of simulated and calculated electrical quantities

		50% S_{rated}	100% S_{rated}	125% S_{rated}
U_{lineHV} [kV]	Simulation	35.7	35.7	35.7
	Calculation	35	35	35
	Deviation [%]	*2*	*2*	*2*
U_{lineLV} [V]	Simulation	388.62	388.62	388.62
	Calculation	400	400	400
	Deviation [%]	*2.8*	*2.8*	*2.8*
I_{HV} [A]	Simulation	2.696	5.19	6.36
	Calculation	2.639	5.28	6.6
	Deviation [%]	*2.11*	*1.7*	*3.63*
I_{LV} [A]	Simulation	230.94	452.36	577.35
	Calculation	234.62	461.88	554.42
	Deviation [%]	*1.59*	*2.06*	*3.97*

3.2.3. Simulation load operation with harmonics

In this study, the harmonic source is modeled using a three-phase bridge-rectifier circuit with thyristors. The harmonic source is directly connected to the 0.4 kV secondary side of the transformer. The firing angle of the thyristors for each operating condition is set as follows: 71° at 50% S_{rated}, 52.5° at 100% S_{rated} and 38° at 125%S_{rated}. After performing the simulation using ANSYS and analyzing the total harmonic distortion (THD) of the voltage (THDu [%]) and current (THDi [%]) in MATLAB, the results obtained from the harmonic distortion are presented in Table 5.

The simulation results reveal that an increase in the firing angle associated with reduced load levels results in a higher THD. Moreover, higher voltage levels are correlated with lower THD values. The harmonic spectrum is shown as Fig. 8, which includes high-order harmonics (5^{th}, 7^{th}, ..., 21^{st}, 23^{rd}, …, 37^{th}, 41^{st}, 43^{rd}). Based on (14) and (15), both the order harmonic and amplitude increase power losses in the transformer; therefore, both facilitate a rise in temperature. This is presented in Section 3.3.

Table 5. Summary of simulation results considering harmonics

		U_p [V]	THDu	I_p [A]	THDi
50%	HV	20786	3.67	2.87	35.29
S_{rated}	LV	232.27	14.62	233.9	38.21
100%	HV	20574	5.64	5.15	28.80
S_{rated}	LV	224.69	24.24	429.6	30.23
125%	HV	20471	6.25	6.52	26.03
S_{rated}	LV	221.04	26.55	560.7	27.16

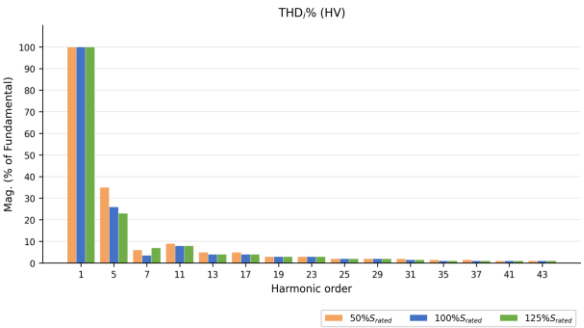

Fig. 8. Harmonic current spectrum of HV winding

The simulation results were validated against analytical calculations performed in Matlab/Simulink, demonstrating a high level of accuracy. Accurate specification and input of material parameters were found to be sufficient for the model to yield loss estimation. This provides a credible foundation for subsequent thermal analyses, including hot-spot temperature evaluation.

3.3. Results of Simulation

Table 6 summarizes the values of P_{NL} and P_{LL} for the two cases, considering and not considering the effect of harmonics, as obtained from the simulations performed in Section 3.2.3.

Table 6. Power loss results

Load	**50% S_{rated}**		**100% S_{rated}**		**125% S_{rated}**	
THDi	0	35.29	0	28.80	0	26.03
P_{dc} [W]	655	986	2550	2884	3870	4650
P_{EC} [W]	30	748	112	1293	170	1120
P_{OSL} [W]	18.4	49.8	18.43	123	18.4	200.6
P_{NL} [W]	250	303	250	305	250	305
P_{LL} [W]	703	1784	2680	4300	4058	5971
P_{LL} [%]	–	254	–	160	–	147

From Table 6, we observe that load losses increase proportionally with the applied load. Furthermore, higher THDi values correlate with increased load losses, ranging from 1.47 to 2.54 times the losses observed without harmonics. Therefore, the top-oil temperature increases very quickly and is much higher than that without harmonics. This is shown in Fig. 9.

Table 5 summarizes the HV/LV voltage and current magnitudes and their total harmonic distortion under different loading levels. At 50% load, the HV voltage magnitude changes only slightly between the sinusoidal and harmonic cases (20.786 kV versus 20.207 kV), i.e., by about 2–3%, and the HV-side voltage distortion remains relatively low, with THDu ≤ 6.25%. In principle, voltage harmonics can make the core flux non-sinusoidal and introduce higher-order flux components, thereby increasing core (no-load) losses. However, Table 6 shows that the no-load loss P_{NL} increases from 250 W to 303–305 W under harmonic conditions (an absolute increase of 53–55 W). Although this is a noticeable relative increase in P_{NL} itself, its contribution is small compared with the dominant load-related losses; when normalized by P_{LL}, the increment corresponds to only 1.37% (50% S_{rated}), 0.62% (100% S_{rated}), and 0.45% (125% S_{rated}).

Therefore, in the investigated cases, the contribution of voltage harmonics to the thermal response is secondary and is neglected in the thermal differential-equation setup; accordingly, the no-load loss is modeled primarily based on the fundamental voltage component. In contrast, Table 6 indicates that current harmonics significantly increase load-related losses, which dominantly drive the observed temperature rise.

In contrast, current harmonics have a much stronger impact on load-related losses, with P_{LL} increasing by approximately 1.47–2.54 times compared with the sinusoidal case (Table 6). This increase in losses leads to higher top-oil and winding temperatures, as shown in Figs. 9-10. Therefore, the subsequent analysis focuses primarily on the thermal impact driven by current harmonics, while voltage harmonics are considered only to justify their comparatively minor contribution under the investigated conditions.

The simulation process is conducted for the three load modes, with each stage lasting 60 min. From the simulation results in Fig. 9, it is clear that the higher the THDi, the faster the oil temperature increases. At t = 60 min, THDi = 35.29%, θ_{oil} increases from 40°C to 70°C. At t = 180 min, θ_{oil} increases from 67°C to 80°C, which is more than 13°C compared with the case without harmonics.

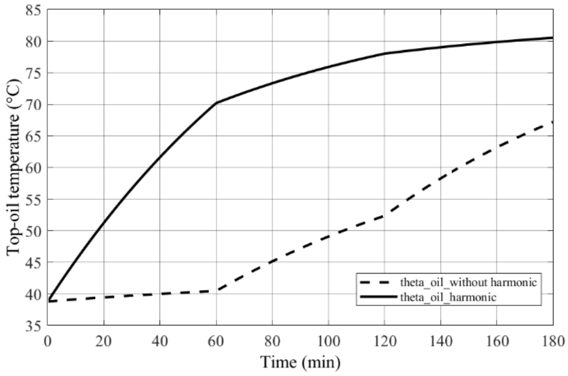

Fig. 9. Top-oil temperature

The comparison of temperatures under nonlinear and linear loads in Fig. 10 clearly assesses the severity of the harmonic waves. For the hot-spot temperature on the winding, there is a significant difference between the pure sine wave load and harmonic load. The largest temperature difference occurs at t = 60 min, reaching 42°C. At 100% S_{rated}, harmonic waves increase the temperature from 77°C to 110°C. For 125% S_{rated} harmonic waves increase the temperature from 102°C to 121°C.

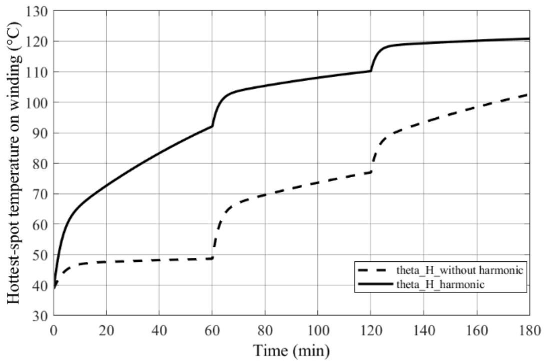

Fig. 10. Hot-spot temperature on winding

Using field plots in ANSYS, the hot-spot region on the winding can be visually localized under both linear (THDi = 0%) and nonlinear (THDi = 26.03%) loading conditions, as shown in Figs. 11–13. The temperature maps indicate a clearly non-uniform thermal field in the winding–core region, where a few localized zones exhibit significantly higher temperatures than the surrounding parts; under harmonic loading, the peak temperature level and the thermal gradient become more severe, making the hot-spot region more critical.

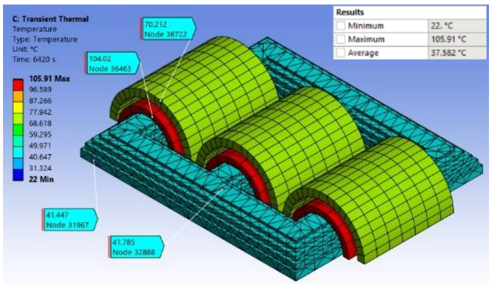

(a)

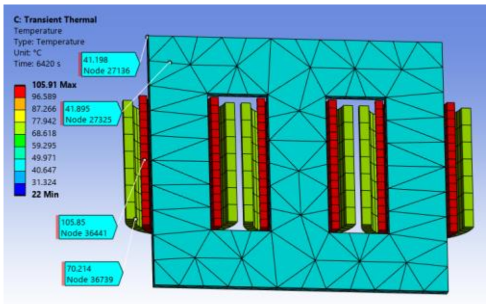

(b)

Fig. 11. Temperature distribution under linear loading at 125% S_{rated} (with THDi = 0%): (a) 3D view of coil and core temperatures; (b) cross-sectional view highlighting the hot-spot location

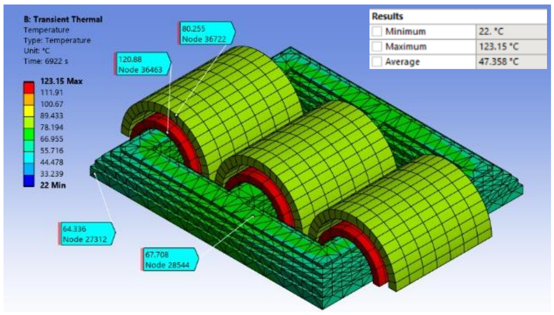

(a)

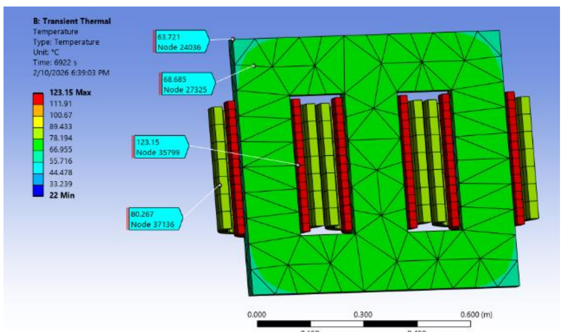

(b)

Fig. 12. Temperature distribution under nonlinear loading at 125% S_{rated} (with THDi = 26.03%): (a) 3D view of coil and core temperatures; (b) cross-sectional view highlighting the hot-spot location

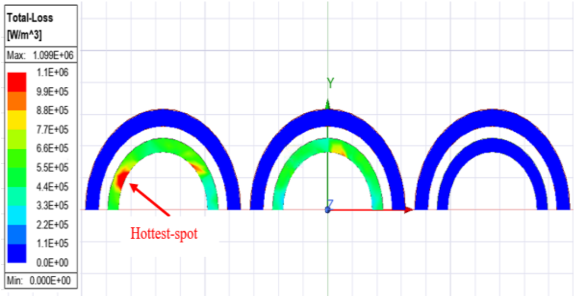

Fig. 13. Hot-spot on low voltage winding when nonlinear load (with THDi = 26.03%)

This spatial information provides practical guidance for *(i)* design improvement, such as targeted reinforcement of insulation and structural adjustments at thermally stressed winding areas; and *(ii)* condition monitoring, by supporting sensor placement at the identified hot-spot locations. From an asset-management perspective, the identified hot-spot regions can support utilities and industrial operators in optimizing periodic inspection and testing of both liquid and solid insulation, prioritizing spare-part planning for thermally stressed components, and implementing more effective condition-based maintenance (CBM) under harmonic operating conditions by integrating dissolved gas analysis (DGA) with complementary fault-diagnosis tools.

To assess the feasibility and efficiency of the proposed hybrid approach, where FEM provides loss inputs and the lumped thermal model rapidly solves the thermal response, we compare the predicted results with detailed thermal simulations in ANSYS Mechanical, as summarized in Table 7. From the comparison results in this Table, the deviation between the analytical formula and the simulation is not large: it is approximately 3% in the linear-load case, whereas it decreases to only 0.016% in the nonlinear-load case. In ANSYS Mechanical, the hottest point is in the middle of the low-voltage winding, while in ANSYS Maxwell, the greatest losses are at the top of the winding, presumably where the temperature is highest. Despite the different locations, the temperature difference between the two points is not too large, less than 1.83%. This shows that the model combining FEM simulation and equivalent circuits, which was calculated from Matlab/Simulink, is reliable enough, and demonstrates the ability to visually observe the uneven distribution and accurately determine the spatial location of the hot-spot on the coil without spending too much setup and calculation time. To ensure more accurate hot temperature location determination, ANSYS Mechanical should be used.

Table 7. Difference between the results of (24) and ANSYS Simulation Mechanics

Hot-spot Temperature on winding	Linear load [°C]	Nonlinear load [°C]
Differential Eq. (24)	102.70	120.90
ANSYS Mechanical	105.91	120.88
Deviation [%]	3.03	0.016

In addition, based on the results shown in Figs. 10 and 13 and the data summarized in Table 8, it can be observed that the increase in hot-spot temperature under harmonic loading significantly accelerates insulation aging and increases the transformer's loss of life. Under the investigated severe operating condition (nonlinear load at 125% overload, cycle duration 120 min), the calculated insulation loss of life over one cycle reaches 66.6 min, compared with 5.031 min under the corresponding linear-load case. This indicates a substantial increase in life consumption under harmonic operating conditions. Consistently, the loss-of-life factor also increases markedly from 0.08385 p.u. (linear load) to 1.11 p.u. (nonlinear load).

Table 8. The loss of lifetime of a transformer

	Linear load	Nonlinear load
Loss of life factor [p.u.]	0.08385	1.11
Load cycle duration [min]	60	60
Loss of life over a cycle [min]	5.031	66.6

Following the validation and thermal-aging analysis discussed above, the parameter values listed in Table 9 are used as inputs to the transformer thermal model to calculate the top-oil and winding hot-spot temperatures via (21) and (24) for the investigated loading cases (50%, 100%, and 125%S_{rated}). The corresponding temperature results are then reported in Fig. 9 and Fig. 10.

Table 9. Parameters input for the transformer thermal model

Quantity	50% S_{rated}	100% S_{rated}	125% S_{rated}
$I_{load\ rated}$ [A]	2.697	5.19	6.36
$I_{load\_harmonic}$ [A]	2.87	5.15	6.52
P_{LL}/P_{NL} at rated	2.812	10.72	16.232
θ_{amb} [°C]		30	
$\Delta\theta_{oil\_R}$ [°C]		38	
n		0.9	
m		0.8	
$\Delta\theta_{oil\_H}$ [°C]		25	
τ_{oil}, min		170	
τ_H, min		6	
$P_{dc\text{-}hotspot}$ [W]	68.8	244	364.95
$P_{EC\text{-}R\_hotspot}$ [W]	30	115	176.7
$P_{EC\text{-}H\_hotspot}$ [W]	32	139.3	292.04

4. Conclusion

This study developed and validated a coupled electromagnetic–thermal framework for evaluating the thermal effects of harmonics in distribution transformers under linear and nonlinear loading conditions. By combining FEM-based electromagnetic loss computation with an equivalent electro-thermal model, the proposed approach enables estimation of top-oil and winding hot-spot temperatures, spatial hot-spot localization, and IEC-based insulation loss-of-life assessment under harmonic operating conditions. The results show that, for the investigated cases, current harmonics are the dominant driver of the observed temperature rise because they significantly increase load-related losses, while the contribution of voltage harmonics to the thermal response is comparatively secondary. In addition, the identified non-uniform temperature distribution and hot-spot regions provide practical value for transformer design refinement (e.g., insulation reinforcement), sensor placement, periodic inspection/testing, spare-part planning, and CBM.

Despite these contributions, the present model still has limitations. In particular, it does not fully account for nonlinear thermal and magnetic material properties, temperature-dependent variations in oil cooling performance, and the detailed thermal behavior of transformer components under severe harmonic excitation. In addition, the current thermal simulation focuses on the winding–core region for hot-spot assessment and does not include the transformer tank. Future work will extend the thermal simulation domain to include the transformer tank and its boundary heat-transfer interactions, enabling a more comprehensive assessment of temperature distribution, hot-spot propagation, and practical cooling/monitoring design under harmonic loading.

References

[1] J. T. Elel, B. Diboma, and A. T. Boum, Transformer's loss of life prediction using a dynamic thermal model, SSRG International Journal of Electrical and Electronic Engineering, vol. 10, no. 2, pp. 44–60, 2023. https://doi.org/10.14445/23488379/IJEEE-V10I2P105

[2] S. Thakur, N. M. Butlero, and J. Holbøll, Effects of harmonics on temperature rise and power loss of a distribution transformer, International Conference on Condition Monitoring and Diagnosis, CMD, Kitakyushu, Japan, pp. 732–735, Mar. 2022. https://doi.org/10.23919/CMD54214.2022.9991585

[3] H. V. Tran and K. A. Nguyen, A Hybrid Ensemble Approach for Dissolved Gas Analysis-Based Power Transformer Fault Diagnosis Using SMOTE and GBDT, Arabian Journal for Science and Engineering, vol. 51, iss. 8, Nov. 2025. https://doi.org/10.1007/s13369-025-10772-z

[4] K. A. Nguyen, H. H. Le, and B. T. Phung, An Adaptive Multi-Fuzzy Logic Model for Diagnosing Transformer Faults Using Dynamic Weight Optimization, e-Prime-Adv. Electr. Eng., Electron. Energy, vol. 13, Jun. 2025, Art. no. 101048. https://doi.org/10.1016/j.prime.2025.101048

[5] M. S. Seddik, M. B. Eteiba, and J. Shazly, Evaluating the harmonic effects on the thermal performance of a power transformer, Energies, vol. 17, no. 19, Sep. 2024, Art. no. 4871. https://doi.org/10.3390/en17194871

[6] J. A. Badri, J.-R. R. Ruiz, A. García, S. Trujillo, and A. Marzàbal, Predicting the effect of voltage harmonic phase angle on transformer core losses. IEEE Transactions on Instrumentation and Measurement, vol. 73, Aug. 2024, Art. no. 6008609. https://doi.org/10.1109/TIM.2024.3449933

[7] Y. Biçen, F. Aras, and H. Kirkici, Lifetime Estimation and Monitoring of Power Transformer Considering Annual Load Factors, IEEE Transactions on Dielectrics and Electrical Insulation, vol. 21, no. 3, pp. 1360–1367, Jun. 2014. https://doi.org/10.1109/TDEI.2014.6832284

[8] D. Susa, M. Lehtonen, and H. Nordman, Dynamic thermal modelling of power transformers, IEEE Transactions on Power Delivery, vol. 20, no. 1, pp. 197–204, 2025. https://doi.org/10.1109/TPWRD.2004.835255

[9] A. Elmoudi, M. Lehtonen, and H. Nordman, Effect of harmonics on transformers loss of life, In Conference Record of the 2006 IEEE International Symposium on Electrical Insulation, Toronto, ON, Canada, pp. 408–411, Jun. 2006. https://doi.org/10.1109/ELINSL.2006.1665344

[10] V.V.s.s. Haritha, T.R. Rao, A. Jain, Thermal Modeling of Electrical Transformers, In Proc. NPSC, Osmania University, Hyderabad, Andhra Pradesh, India, pp. 597-602, Dec. 2010.

[11] D. D. Maio and T. Tinga, Transformer Hot Spot Temperature Prediction Based on Basic Operator Information, International Journal of Electrical Power & Energy Systems, vol. 124, Jan. 2021, Art. no. 106340. https://doi.org/10.1016/j.ijepes.2020.106340

[12] J.-M. Jin, The Finite Element Method in Electromagnetics, 3rd ed., Wiley–IEEE Press, 2014.

[13] IEEE Recommended Practice for Establishing Liquid Immersed and Dry-Type Power and Distribution Transformer Capability when Supplying Nonsinusoidal Load Currents, IEEE Std C57.110-2018, 2018.

[14] Power transformers–Part 7: Loading guide for mineral-oil-immersed power transformers, IEC 60076-7, 2018.

[15] G. Swift, T. Molinski, and W. Lehn, A fundamental approach to transformer thermal modeling–Part I: Theory and equivalent circuit, IEEE Transactions on Power Delivery,, vol. 16, no. 2, pp.171–175, Apr. 2001. https://doi.org/10.1109/61.915478